Large bulk matter search for fractional charge particles

Irwin T. Lee, Sewan Fan, Valerie Halyo, Eric R. Lee, Peter C. Kim, Martin L. Perl, and Howard Rogers
Stanford Linear Accelerator Center, Stanford University, Stanford, California 94309

Dinesh Loomba
Department of Physics, University of New Mexico, Albuquerque, New Mexico 87131

Klaus S. Lackner
Department of Earth and Environmental Engineering, Columbia University, New York, New York 10027

Gordon Shaw
Department of Physics, University of California–Irvine, Irvine, California 92717

We have carried out the largest search for stable particles with fractional electric charge, based on an oil drop method that incorporates a horizontal electric field and upward air flow. No evidence for such particles was found, giving a 95% confidence level upper limit of 1.17×10^{-22} particles per nucleon on the abundance of fractional charge particles in silicone oil for $0.18e \leq |Q_{residual}| \leq 0.82e$. Since this is the first use of this new method we describe the advantages and limitations of the method.

I. INTRODUCTION

We have carried out the largest search for fractional electric charge elementary particles in bulk matter using 70.1 mg of silicone oil. That is, we looked for stable particles whose charge Q deviates from Ne where N is an integer, including zero, and e is the magnitude of the charge on the electron. No evidence for such particles was found in this amount of silicone oil. We used our new version [1] of the Millikan oil drop method containing two innovations compared to the classical method that we used in Halyo *et al.* [2]. One innovation is that the drop charge is obtained by observing the drop motion in a *horizontal*, alternating electric field compared to the classical use of a vertical electric field [2–4]. The other innovation is the use of an upward flow of air to reduce the vertical terminal velocity of the drop, which enabled us to use larger drops, about 20.6 μm in diameter compared to the 10 μm drops used in our previous experiments.

We define the residual drop charge, $Q_r = Q - N_l e$ where N_l is the largest integer less than Q/e. We find the 95% confidence level upper limit on the abundance of fractional charge particles in silicone oil for $0.18e \leq Q_r \leq 0.82e$ is 1.17×10^{-22} particles per nucleon. This experiment was a follow up on our previous search in silicone oil, Halyo *et al.* [2], based on 17.4 mg. In that search we found one drop with anomalous charge, but no such charge was found in the present experiment.

In this paper we describe the experimental method and apparatus in Sec. II. In Sec. III we discuss the measurement precision resulting from the various measurement errors and the calibration methods. The data analysis method, including the criteria used to accept drop charge measurements, is discussed in Sec. IV. Here we pay particular attention to the drop spacing criterion necessitated by interactions between adjacent drops. This is the primary limitation on the rate at which drops can be measured and we had to acquire considerable experience to understand this limitation. We conclude with Sec. V, giving our results, comparing our results with other fractional charge searches, and discussing the applicability and extension of this new Millikan oil drop technique to other searches.

II. EXPERIMENTAL METHOD AND APPARATUS

A. Experimental method

The principle of the experimental method is simple. Consider a drop of radius r, density ρ, and charge Q falling in air through a horizontal electric field of strength E, as shown in Fig. 1. Applying Stokes's law the horizontal terminal velocity, v_x is

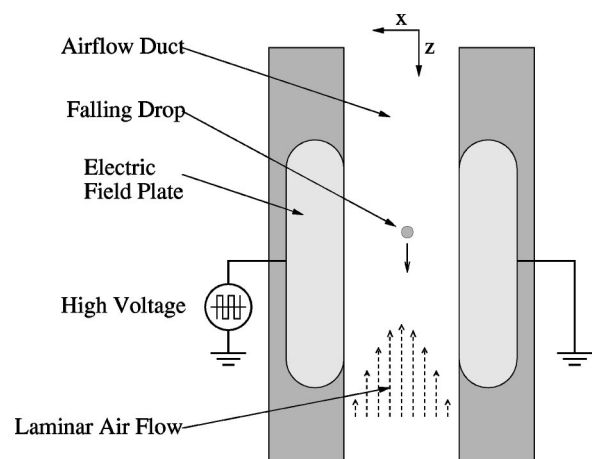$$v_x = \frac{QE}{6\pi\eta r} \qquad (1)$$

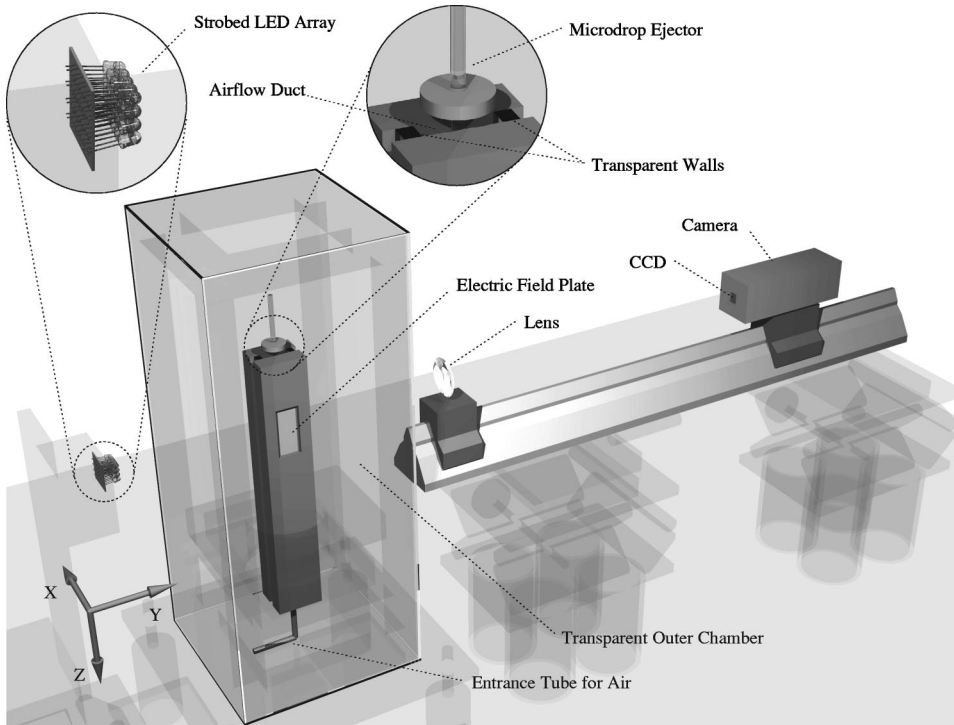FIG. 1. Basic principles of the experimental method.

FIG. 2. Diagram of the apparatus. Diagram is to scale, except for the lens and CCD which are shown at 2× scale. Support structures are drawn transparent for clarity.

where η is the viscosity of air. Hence measuring v_x gives Q providing r is known. As explained in Sec. III A, the drop radius is determined from the v_x of integer charge particles. Note that the measurement of Q does not depend on the density of the drop and is also independent of the gravitational force on the drop. The electric field alternates in the $+x$ and $-x$ direction so that the drop is moved back and forth along the x axis. This cancels some sources of error and allows the drop motion to be viewed in a relatively narrow horizontal area. Previous uses of a static horizontal electric field in the Millikan oil drop method were in 1941 by Hopper and Laby [5] who measured the electron charge and by Kunkel [6] in 1950 who measured the charge on dust particles.

If the drop were falling in still air, the vertical terminal velocity would be given by

$$v_{z,term} = \frac{2r^2 \rho g}{9\eta} \qquad (2)$$

where g is the acceleration of gravity. However we use an upward flow of air of velocity v_{air} in the $-z$ direction. Hence the net downward velocity of the drop is

$$v_z = \frac{2r^2 \rho g}{9\eta} - v_{air}. \qquad (3)$$

As explained in the next section we want v_z to be small hence we set v_{air} to be close to $v_{z,term}$ but slightly smaller.

B. General description of experiment

Figure 2 is a schematic picture of the apparatus. Drops averaging 20.6 μm in diameter are produced at a rate of 1 Hz using a piezoelectrically actuated drop-on-demand micro-

drop ejector. The drops fall through the upward moving air in the measurement chamber passing through a horizontal, uniform, alternating electric field. In this figure the electric field is perpendicular to the paper. The electric field alternates as a square wave with a frequency of 2.5 Hz and has an amplitude of about 1.8×10^6 V/m.

A rectangular measurement region 2.29 mm in the x direction by 3.05 mm in the z direction is projected by a lens onto the charge-coupled device (CCD) sensor of a monochrome, digital video camera. A light source consisting of a bank of light emitting diodes (LEDs) provides 10 Hz stroboscopic illumination. As the motion of the drop carries it through the measurement region, its image appears on the surface of the CCD. Thus the camera collects 10 frames per second, the drop appearing as a dark image on a bright background.

In addition to the v_x motion there is also the v_z motion, Eq. (3). Since the camera has a field of view of $Z = 3.05$ mm in the vertical direction, the 10 Hz stroboscopic illumination leads to acquisition of

$$N_{images} = 10Z/v_z = 30.5/v_z \qquad (4)$$

images of any given drop, before the drop moves below the viewing area of the camera. Here v_z is in mm/s. Hence we get a larger number of images per drop, leading to better charge measurement precision, when v_z is small. Of the order of $N_{images} = 15$ are required.

We give an example of the importance of the upward airflow in obtaining this many images. Consider a typical drop of diameter 20.6 μm with a density of 0.913 g/cm^3. From Eq. (2), $v_{z,term} = 11.3$ mm/s. If there were no upward airflow there would be an average of 2.6 images per drop. To obtain $N_{images} = 15$, v_z must be about 2.0 mm/s. Therefore
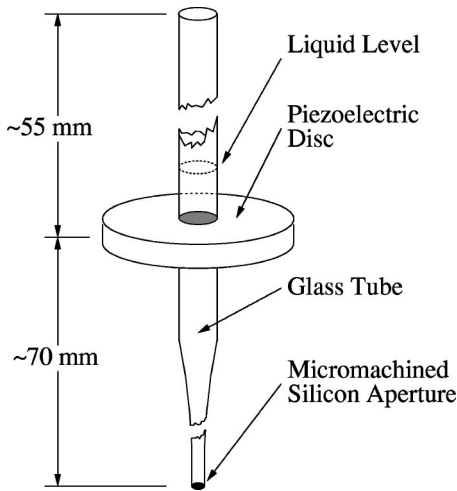
FIG. 3. Drop generator.

from Eq. (3), v_{air} must be $11.3 - 2.0 = 9.3$ mm/s.

Each image from the CCD camera is processed though a framegrabber in a conventional desktop computer, the signal in each pixel being recorded. An analysis program then finds the drop images and calculates the x and z coordinates of the centroid of the drop image. Using all the images of the drop and knowing the time spacing of the images, v_x and v_z are then calculated.

C. Drop generator

The drop generator, Fig. 3, is based on the general design principles used in piezoelectrically actuated, drop-on-demand, inkjet print heads. Our generator is designed for flexibility, allowing a variety of liquids to be used and providing ease of control and maintenance. The body of the generator is glass so as to preserve the purity of the liquid, but the ejection aperture at the bottom is micromachined silicon [7]. The diameter of the aperture sets approximately the diameter of the drop. Upon application of a short voltage pulse, usually 3 to 20 μs, across the surfaces of the piezoelectric disk, the central hole in the disk contracts in diameter, squeezing the glass tube and sending a pressure pulse down the liquid, ejecting a jet of fluid from the aperture. The forming of a discrete fluid drop from the high speed jet is a complex process with the repeatability of the process and the final diameter of the drop being highly dependent on the properties of the fluid, and on how the fluid is driven. For this reason, the shape and amplitude of the voltage pulse applied to the piezoelectric disk must be specifically tuned for stability and the desired drop size. In addition, it is necessary to experiment with single and double pulsing, varying both the pulse width and the separation between the pulses.

The pressure in the drop generator is maintained slightly below atmospheric pressure by 10 to 30 mm Hg. This helps to retract the excess liquid outside the ejection aperture after the drop has been produced and also prevents leaking of the liquid between pulses.

It is important that the drop generator produce drops of constant radius, the primary reason being that the size of the

drops determines the ratio between Q and the measured quantity v_x, from Eq. (1). A secondary reason that we did not initially appreciate has to do with Eqs. (2) and (3). We set v_{air} close to $v_{z,term}$ so that v_z is much smaller than $v_{z,term}$. Thus a small change in r leads to a relatively large change in v_z. This dispersion disrupts the consistent spacing between adjacent drops, and a decreased separation between drops is undersirable for reasons discussed in Sec. IV A 6.

With a clean and newly tuned drop generator we get remarkably uniform drop radii, constant to about $\pm 0.2\%$. The drop generator also ejects in a consistent downward vertical direction along the centerline of the airflow tube. At 1 Hz operation, the drop ejector exhibits slow drifts in its characteristics with time scales of the order of a week. These drifts appear as changes in drop size and as destabilization that manifests as the appearance of satellite drops or inconsistent drop production. Typically, these effects can be compensated for by small changes in the drive parameters or adjustments of the air velocity or both. By the end of the first data set, set 1, the drop ejector had destabilized to the point where it had to be removed from the apparatus for cleaning and refilling. Similarly during the taking of data set 2, the drop ejector and air velocity required periodic small adjustments. The end of set 2 was caused by increasing instability in drop production which could not be compensated for. We do not know the reason for this behavior.

In our drop generator the silicone oil drops are produced with a spread of charges, $|Q|$ ranging mostly from 0 to about 10 e. A few percent of the drops have larger $|Q|$. As described in Sec. IV A 1 we used drops with $|Q| < 9.5e$ to maintain good precision in the charge measurement. We do not know what sets the charge distribution for a particular drop generator. But we have the general observation that silicone oil gives narrow charge distributions, whereas water, mineral oil and most other organic liquids give broad charge distributions, with $|Q|$ values as large as several 1000 e or even larger.

D. Optical system

Referring to Fig. 2, the stroboscopic light source consists of a rectangular bank of 20 LED's emitting at 660 nm. The pulse length was about 100 μs. The lens, a 135 mm focal length, $f/11$, photographic enlarging lens, images the measurement region onto the face of the CCD camera with a magnification of 2.1.

The rectangular active image area of the CCD camera [8] is 4.8 mm in the horizontal, that is, x, direction, and 6.4 mm in the vertical, that is, z, direction. Hence the viewing area in physical space is 2.29 mm horizontally by 3.05 mm vertically. We remind the reader that the electric field is horizontal. The active imaging area is an array of 240 horizontal picture elements (pixels) and 736 vertical picture elements (pixels). We chose this orientation of the array to maximize the vertical distance, maximizing the number of images per drop.

Given the magnification and pixel density of the CCD, one would expect from geometric optics that the shadow of a 20 μm diameter drop would cover 2 pixels horizontally and
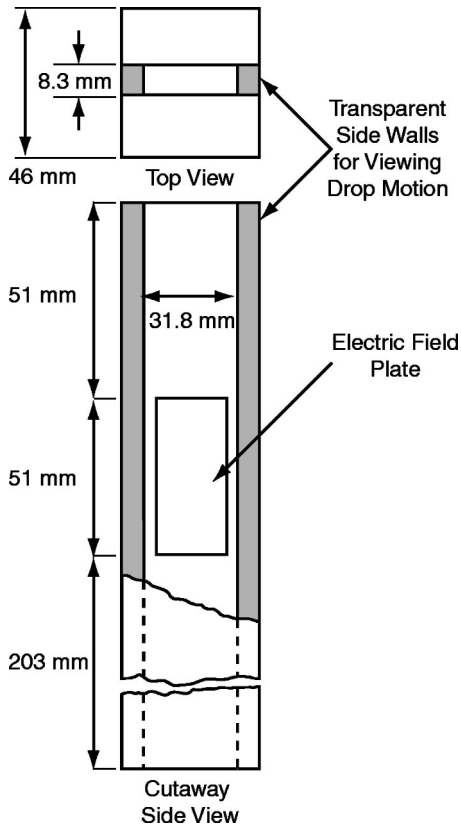
FIG. 4. Airflow tube and measurement chamber.

5 pixels vertically. The actual observed shadow typically covered 3 pixels horizontally and 7 pixels vertically, and had an intensity variation that was approximately a two dimensional Gaussian. This can be quantitatively described as the convolution of the simple shadow predicted by geometric optics with a point spread function that is a result of the diffractive effects due to the finite aperture of the lens. We do not and should not observe diffractive effects caused by the small size of the drops.

E. Airflow tube and measurement chamber

Figure 4 shows a slightly simplified, dimensioned drawing of the airflow tube and the measurement chamber. A rectangular duct contains the upward flowing air. It is 8.3 mm wide in the direction of the electric field and 31.8 mm wide in the direction perpendicular to the electric field. The field plates that define the measurement chamber are 51 mm high and 28.6 mm wide. The inner surfaces of the plates are machined flat and are in the same plane as the inner surfaces of the walls of the airflow tube. The optic axis of the optical system passes through the transparent side walls of the airflow tube.

The air velocity is sufficiently small, with a Reynolds number on the order of $R_e = 50$ so that the flow is laminar. The 203 mm length of air flow tube between the measurement region and the air inlet allows the air to settle into its equilibrium flow pattern. At equilibrium, the velocity profile of the air is approximately parabolic across the narrow direction of the channel (x axis). Across the long axis, the flow

has a roughly constant central region and falls to zero at the boundaries [9].

F. Electronics

All the electronics of the apparatus, Fig. 5, are hard-wired to give reliable timing, independent of the operation of the computer. A 30 Hz handshaking signal from the CCD is divided down to provide a 10 Hz clock that synchronizes the LED strobe, the electric field switcher and the computer image acquisition. The switching of the electric field, which is driven by the clock signal divided by 4, operates at 2.5 Hz. This results in a cycle where two images are acquired with the electric field in one direction, and then two images with the electric field in the other direction. These relationships between the signals is depicted in the timing diagram of Fig. 5. The drop generator is driven asynchronously at 1 Hz.

G. Data acquisition and storage

Data acquisition was performed by a single desktop computer running Linux. The computer was equipped with two special components: a digital framegrabber that allowed the capture of image data from the camera and a general purpose input/output interface board with digital I/O and A/D conversion capability. The additional inputs allowed the computer to monitor the state of the experiment as well as a variety of environmental variables.

All software was custom written in C. Hardware dependent code was encapsulated into drivers at the kernel level, which allowed a guarantee of synchronization of the software with apparatus by a combination of hardware and software buffering of the data.

The overall strategy was to acquire data from the apparatus and write them to files in *raw* form for later processing off line. Recall that each image frame contains 736×240 pixels, each digitized to 8 bit accuracy. Therefore acquiring data at 10 Hz produces a data rate from the CCD camera of about 2 MB/s, much too large to be stored. Since an image contains just a few drops, most of the pixels in an image have just the background signal, which allows the information to be stored using sparse storage. As mentioned in Sec. II D, the typical image of drop extends over an area of 3 pixels by 7 pixels. In each frame the regions containing drops were isolated using a thresholding operation. The position of each drop was then measured using a simple center of mass algorithm, and for each drop only a surrounding region containing 13 horizontal pixels by 21 vertical pixels of the image is written to the output file.

H. Data collection

The search was carried out in two sets described in Table I. At the beginning of the set 1 the drop ejector was operated at 0.5 Hz, then at 1 Hz for the remainder of set 1 and all of set 2.
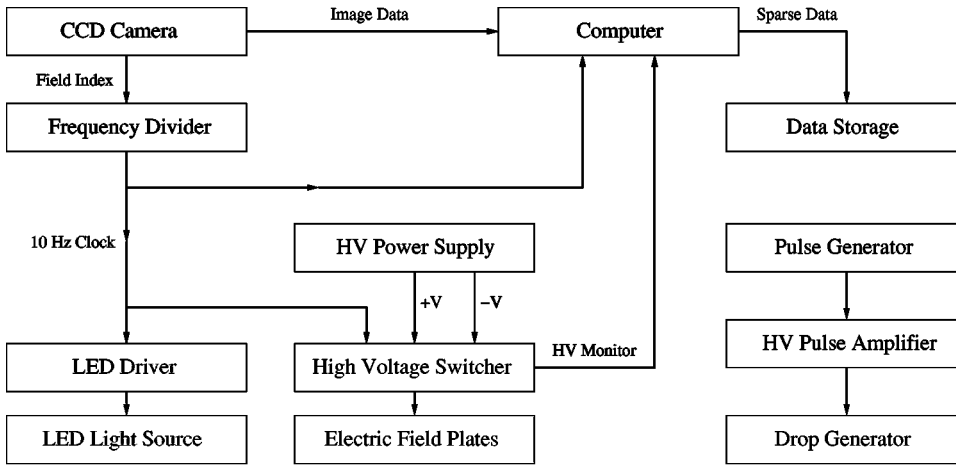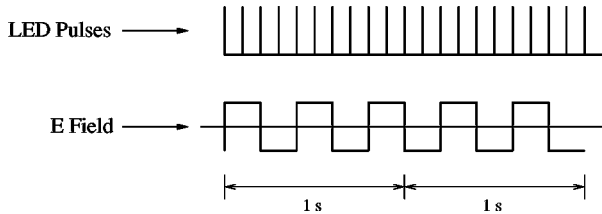
FIG. 5. Schematic of electronic system. The LED and high voltage is synchronized to the 10 Hz clock, while the drop generator runs asynchronously.

III. CALIBRATION, ERRORS, AND MEASUREMENT PRECISION

A. Electric field and drop radius

Rewrite Eq. (1) in the form

$$v_x = \left(\frac{Q}{6\pi\eta}\right)\left(\frac{E}{r}\right). \tag{5}$$

Consider nonfractional values of $Q = ne$, $n = 0, \pm 1$, $\pm 2, \ldots$. Then, as shown in Sec. IV B, the measured values of v_x sharply peak at $n = 0, \pm 1, \pm 2, \ldots$. From a fit to the center of these peaks, Eq. (5) gives the fitted E/r ratio.

The electric field strength, E, is calculated from the measured voltage across the electric field plates, known to 3%, and the plate separation, 8.25 ± 0.01 mm. The plates are parallel to within 0.1 mrad. Inserting the calculated value of E into the fitted E/r ratio, we obtain the drop radius r.

We have two additional checks of the drop radius, one from the measurement of the error caused by the Brownian motion, Sec. III B, and the other from the measurement of the net downward velocity of the drops, v_z in Eq. (3).

The drop radius depends to a moderate extent upon the size and shape of the voltage pulse applied to the drop generator and to a slight extent upon the age and history of the drop generator. However over periods of hours the average drop radius could be taken to be constant, with fluctuations of $\pm 0.2\%$ for individual drops. Since the data were analyzed

in one-hour-long blocks, the average E/r ratio for any given block was known to much better accuracy than this.

B. Brownian motion and drop position measurement errors

The precision of the determination of the drop charge depends upon the precision of the measurement of v_x. Consider the sequence of position measurements x_i of the trajectory of a drop. For two consecutive frames, j and $j-1$, the velocity measurement $v_{x,j}$ is given by

$$v_{x,j} \equiv \frac{x_j - x_{j-1}}{\Delta t}. \tag{6}$$

Here, Δt is the time between successive frames, 0.1 s in our case. Since Δt is known with very good precision, the error in measuring v_x comes from the error in determining the x_i of the drop centers, and from Brownian motion. Take the error in centroiding to be normally distributed with a standard deviation of σ_c.

During the time Δt between any two successive measurements of the x_i positions, Brownian motion adds a random contribution with standard deviation (std. dev.) given by

$$\sigma_b = \sqrt{\frac{kT\Delta t}{3\pi\eta r}}. \tag{7}$$

Here k is the Boltzmann constant, T is the absolute temperature, η is the viscosity of air and r is the drop radius.

The trajectory of uncharged drops, which have no contribution to their trajectories due to the electric field, can thus be written as

$$x_j = x_0 + \sigma_{c,j} + \sum_{i=1}^{j} \sigma_{b,i}$$

TABLE I. Data collection.

Data set	Weeks	Number of drops	Total mass (mg)
1	13	3 377 477	12.1
2	17	13 430 167	58.0

$$j = 1, 2, \ldots, N_{images} \qquad (8)$$

with x_0 set by the initial position of the drop, and where the $\sigma_{c,i}$ ($\sigma_{b,i}$) are normally distributed with a std. dev. of σ_c (σ_b). The analysis for charged drops is similar if the effect of the electric field is first subtracted from the observed data points. It then follows that

$$v_{x,j} \Delta t = \sigma_{b,j} + \sigma_{c,j} - \sigma_{c,j-1} \qquad (9)$$

and

$$\langle v_{x,j} v_{x,k} \rangle \Delta t^2 = \begin{cases} 2\sigma_c^2 + \sigma_b^2, & j = k, \\ -\sigma_c^2, & |j-k| = 1, \\ 0 & \text{otherwise.} \end{cases} \qquad (10)$$

Therefore the total error on any given velocity measurement, σ_v, is given by $\sigma_v^2 = 2\sigma_c^2 + \sigma_b^2$, and the centroiding error introduces an anticorrelation with magnitude $-\sigma_c^2$ in two consecutive velocity measurements, due to the shared position measurement. We use the concept summarized in Eq. (10) and the observed distributions of the $v_{x,i}$ (after removal of the contribution due to the alternating electric field) to separate σ_c from σ_b.

We find that averaged over this experiment,

$$\sigma_c = 0.31 \ \mu\text{m}, \qquad \sigma_b = 0.47 \ \mu\text{m}, \qquad (11)$$

in the measurement region. Compared to the size of an individual pixel on the CCD, the centroiding error is small, approximately 1/30 of a pixel. The value of σ_b obtained provides an independent check on the size of the drops, and is consistent with the size determined from the terminal velocity and the electric field drift velocity.

Equation (11) shows that the Brownian motion error, σ_b, is about the same magnitude as the error involved in finding the drop position, σ_c. Therefore substantially reducing σ_c through the use of smaller pixels will not by itself substantially reduce the error on the charge measurement, since the Brownian motion error can only be reduced by increasing N_{images}.

The final charge measurement of a drop is made using a single, detailed best fit to the entire observed trajectory of the drop, and the final error on the charge measurement σ_q is a result of propagating the errors σ_c and σ_b through this calculation.

C. Other sources of errors

We looked for other sources of errors, but all are negligible compared to those in Eq. (10). When we developed the upward air flow method we thought about the possibility that there might be some horizontal air velocity, $v_{x,air}$ in the measurement chamber, contributing an error to σ_v of order $v_{x,air} \times \Delta t$. By studying a large amount of data we found that the distribution of $v_{x,air} \times \Delta t$ had an rms value of 100 nm, and was a fixed property of the measurement region. For comparison $v_e \times \Delta t$ was of the order of 8 μm. These irregularities in $v_{x,air}$ are probably due to residual surface imper-

TABLE II. Drop selection criteria. The entries are the percent removed by each criterion separately. The bottom row gives the total percent of drops removed by all criteria. Since the same drop may be removed by several criteria, the total percent removed is *not* the sum of the percent removed by the individual criteria.

Criterion	Set 1	Set 2
q	0.3	0.6
σ_q	4.1	0.6
χ^2	4.9	2.5
v_z	4.6	4.0
x	9.3	0.5
R	12.4	5.4
Total	21.0	9.4

fections in the electric field plates. Since the irregularities are constant over long periods of time, they can be accurately measured and corrected for. For this analysis, that was not necessary.

Another possible source of error would be a nonuniformity in the electric field in the measurement region giving a horizontal gradient, dE/dx. This would produce a horizontal force on the drop's induced electric dipole moment. This dipole force acts in addition to the QE force. We found such a dipole force to be negligible compared to the QE force.

A small, vertical deceleration of the drops as they fall through the measurement chamber was observed. This amounted to a change of 30 μm/s in the apparent terminal velocity of the drops as they fell through the measurement region, or a systematic uncertainty in the radius of the drop of the order of 0.3%. We believe that the deceleration is due to the evaporation of the drop as it falls. The magnitude of this effect is small enough such that it can be neglected in the calculation of v_x. As a side note, any systematic uncertainties in the radius of the drops are absorbed by the calibration process described in Sec. III A, and do not affect the final charge measurement.

Similarly, other possible sources of measurement error such as apparatus vibrations, optical distortions and CCD array distortions, and patch nonuniformities on the electric field plates, were negligible.

IV. DATA ANALYSIS AND RESULTS

A. Drop selection criteria

In this section we use $q = Q/e$, a measure of the drop charge in units of the electron charge. We required that all drops used in the analysis meet the criteria in Table II. The criteria are designed to maintain a charge measurement accuracy of approximately 0.03 e and to reject irregular drops caused by inconsistent operation of the drop generator.

1. q<9.5 criterion

For any given drop there is an uncertainty in the radius of approximately 0.2% which contributes to the relative error on q. The *absolute* error on q thus increases linearly with q. Since the absolute error on q must be kept to the order of

0.03 e, restricting the data sample to drops with $q<9.5$ keeps this contribution to less than 0.02 e. The overall charge distribution is such that only a few percent of the drops have q values outside this range.

2. $\sigma_q < 0.03$ criterion

Primarily, this criterion is a measure of N_{images} of the drop. Brownian motion and centroiding accuracy, characterized by σ_c and σ_b as described in Sec. III B, limit the accuracy of the charge measurement, σ_q. For any given drop, the number of position measurements, N_{images}, and the state of the electric field during those measurements, in addition to σ_b and σ_c, determines this accuracy. As noted earlier, N_{images} was of the order of 15. If a drop has an exceptionally large radius or is falling too far from the centerline of the airflow tube, v_z will be too large and N_{images} will be too small.

3. χ^2 criterion

As mentioned earlier, the final calculation of the charge on a drop is done using a fit to the trajectory of the drop. It was required that the χ^2 probability of the fit to the drop's trajectory be better than 10^{-3}. This rejects a large class of rare artifacts based on the statistical likelihood that the observed deviations from the fitted trajectory could be attributed to the Brownian motion and centroiding errors. For example, a drop would be rejected if it had an anomalous trajectory due to vibrations in the apparatus or due to its charge having been changed by collision with an ion during measurement.

4. v_z criterion

The net downward velocity of the drop, v_z, depends upon the drop radius and the upward air velocity, v_{air}, Eq. (3). This criterion insures consistent drop radii within the hour long data blocks by requiring

$$|v_{z,drop} - v_{z,block}| < 0.124 \;\; \text{mm/s} \tag{12}$$

where v_z is the measured value for one drop and $v_{z,block}$ is the average value of v_z for all the drops in the one hour data block. Using Eqs. (2) and (3), taking v_{air} as fixed and using an average value for r of 10 μm, this eliminates any drops with r different from the nominal value by more than about $\pm 0.5\%$.

Recall that the air velocity is approximately parabolic and that close to the centerline it is given by

$$v_{air}(x) = v_{air,0}[1 - (x/x_w)^2] \tag{13}$$

where x is the distance along the x axis from the centerline of the airflow tube, $x_w = 4.15$ mm is the distance to the wall of the tube, and $v_{air,0}$ is the air velocity along the centerline. Therefore this criterion indirectly restricts how far the drop can be from the centerline.
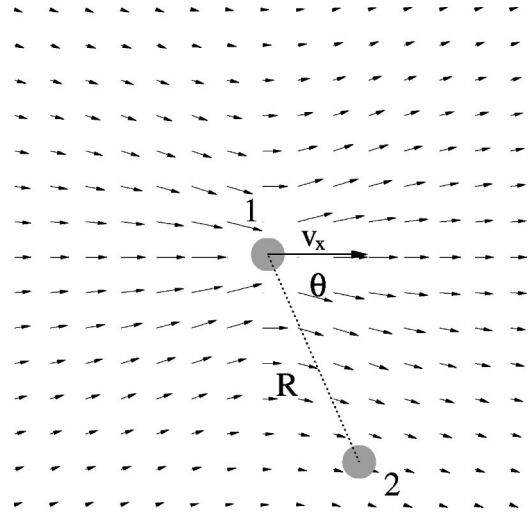

FIG. 6. The viscous coupling between a moving drop 1 on a neighboring drop 2 in still air. The small arrows show the vector velocity of the disturbed air. Note that there is a slight disturbance at the position of drop 2 that will affect the trajectory of drop 2.

5. x deviation criterion

This criterion

$$|x - x_{block}| < 0.19 \;\; \text{mm} \tag{14}$$

provides a direct constraint on how far a drop may deviate from the centerline in the x direction. Here x_{block} is the average value of x for all the drops in the one hour data block. The purpose of this criterion is to eliminate drops that were produced irregularly. The 0.19 mm upper limit in Eq. (14) was determined by examining the distribution of x positions of drops produced during normal operation of the drop generation and setting the upper limit to eliminate the tails.

6. Minimum distance R between any two drops criterion

The drops interact with one another through their induced electric dipole moments and viscous coupling through the air. Consider two drops of radius r, drop 1 moving with a velocity v_x due to the force of the electric field on its charge, as shown in Fig. 6. This motion will move the surrounding air. At the position of drop 2, the velocity of the air in the x direction, $V_{x,\text{disturbed air}}$, is given by

$$V_{x,\text{disturbed air}} = \frac{3}{4} \frac{v_x r}{R} (1 + \cos^2\theta). \tag{15}$$

Since drop 2 sits in this disturbed air, its v_x due to the force of the electric field on its charge will have superimposed upon it $V_{x,\text{disturbed air}}$. This will distort the charge measurement. Therefore $V_{x,\text{disturbed air}}$ must be kept small by keeping R, the distance between the drops, much larger than r, the radius of the drop. A large separation also serves to minimize the interaction between the induced electric dipole moments of the drops, which increases as the inverse fourth power of the separation. We require
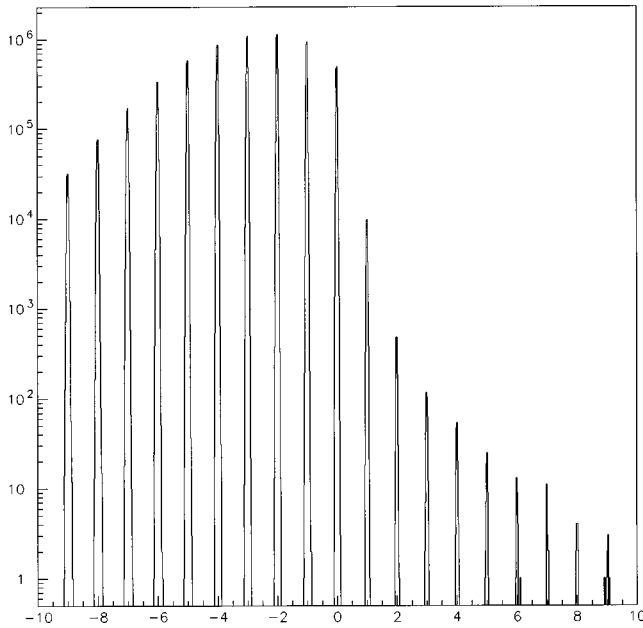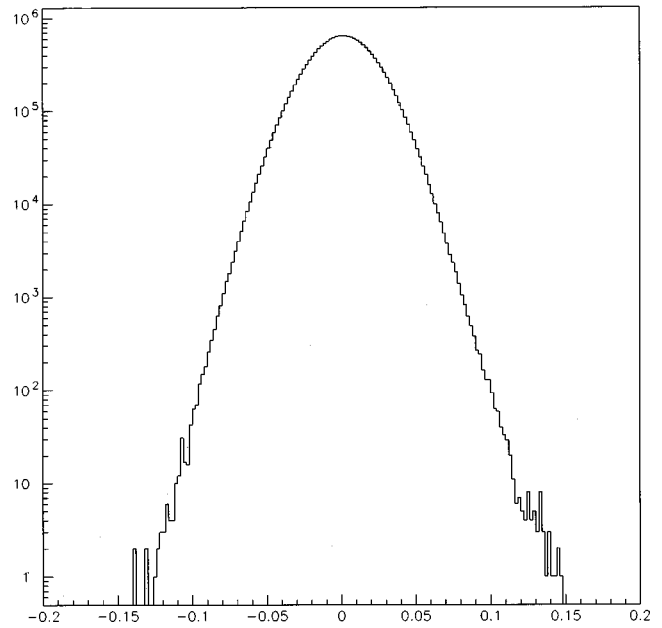
FIG. 7. The q charge distribution in units of e.

FIG. 8. The q_c charge distribution in units of e.

$$R > 0.62 \text{ mm} \tag{16}$$

separation between any two drops, which limits these forces to a small fraction of QE.

7. Summary and magnitude of drop selection criteria

Table II gives the percent of drops removed by each criterion averaged over each of the two data sets. The total percent of drops removed is also given. Since the same drop may be removed by several criteria, the total percent removed is *not* the sum of the percent removed by the individual criteria.

B. Results

After the application of these criteria we had a final data sample of 1.7×10^7 drops of average diameter 20.6 μm. The total mass of the sample was 70.1 mg. Figure 7 shows the charge distribution in units of e. (The asymmetry of the charge distribution is a property of the drop generator as discussed in Sec. II C.) We see sharp peaks at integer numbers of charges and no drops further than 0.15 e from the nearest integer. We emphasize that there is no background subtraction here; this is all the data after the application of the criteria previously discussed.

To show the shape of the peaks at integer values of q we superimpose them in Fig. 8 using the charge distribution, q_c, defined by $q_c = q - N_c$ where N_c is the signed integer closest to q. The peaks have a Gaussian distribution with a standard deviation of 0.021 e. *The absence of non-Gaussian tails is what allows this search method to be so powerful.*

In Fig. 9 we superimpose the valleys between the peaks using the residual charge distribution, q_r, defined by $q_r = q - N_l$ where N_l is the largest integer less than q. We did not find any drops with residual charge between 0.15 e and

0.85 e. In this residual charge range there are fewer than 1.17×10^{-22} fractional charge particles per nucleon in silicone oil with 95% confidence.

Thus this 70.1 mg search did not confirm the one unusual aspect of our previous 17 mg search, Halyo *et al.* [2], where we found 1 drop with a q_r of about 0.29 e. No such charge was found in this search. While it is of course still possible that the fractional charge found in the 17 mg experiment was real, we are inclined to believe that the 17 mg experiment had a very small background that has been eliminated by the improved method of this experiment.
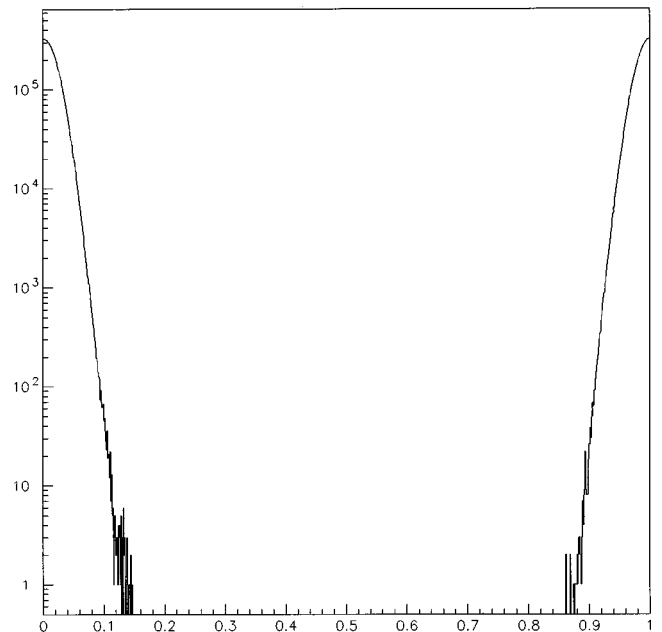

FIG. 9. The q_c residual charge distribution in units of e.

TABLE III. Searches for fractional charge particles in ordinary matter. All experimenters reported null results except LaRue *et al.* [10]. There are 6.4×10^{20} nucleons in a milligram.

Method	Experiment	Material	Mass (mg)
levitometer	LaRue *et al.* [10]	niobium	1.1
levitometer	Marinelli *et al.* [11]	iron	3.7
levitometer	Smith *et al.* [12]	niobium	4.9
levitometer	Jones *et al.* [13]	meteorite	2.8
liquid drop	Halyo *et al.* [2]	silicone oil	17.4
liquid drop	this search	silicone oil	70.1

V. CONCLUSIONS

A. Comparison with other fractional charge searches in bulk material

In Table III we compare this search with previous, larger sample, searches for fractional charge particles in bulk matter. No evidence for fractional charge particles was found in the searches by Marinelli *et al.* [11], Smith *et al.* [12], and Jones *et al.* [13], similar to the null result in the present search.

In their superconducting levitometer search in niobium, LaRue *et al.* [10] claimed to have fractional charge particles with $e/3$ and $2e/3$. But Smith *et al.* [12] who also searched in niobium using a ferromagnetic levitometer method did not find any such evidence in a four times larger sample. At present the results of LaRue *et al.* [10] are not understood and are generally not accepted.

Our search is by far the largest to date and has the smallest upper limit of any search on the concentration of fractional charge particles in bulk matter. But it is important not to generalize our limit to other kinds of bulk matter for several reasons. First, we do not know what happens to fractional charge particles that are in natural matter when that matter is processed. Note that except for the search in meteoritic material by Jones *et al.* [13], all the material in Table III is processed.

Second, if we assume the existence of stable, fractional charge particles, we do not know what natural materials are most likely to have a detectable concentration. Our own thoughts are that the most promising natural material is that found in carbonaceous chondrite asteroids, since they are representative of the primordial composition of the solar system, having not undergone any geochemical or biochemical processes. Hence similar to the motivation of Jones *et al.* [13], our next search will be in meteoritic material from an asteroid.

B. Remarks on further use of this new method

The purpose of the new method [1] used in this experiment was to allow large drops to be used compared to the classical method, thus increasing the rate at which we could search through a sample and also enabling the use of suspensions of more interesting materials. We have succeeded in doing this, using drops of about 20 μm diameter compared to the approximately 10 μm diameter used in Halyo *et al.*

[2]. In the Appendix we discuss further increasing the search rate by using still larger drops and by using multiple columns of drops to increase the total rate of drop production. We find that with this new method the mass per second search rate can be further increased by a factor of the order of 10, but probably not by a factor of 100.

APPENDIX: INCREASING THE SEARCH RATE

There are several ways in which the mass per second search rate can be increased in this experimental method.

1. Use of larger drops

The first way to increase the search rate is to use larger drops. Maintenance of the precision of the charge measurement requires that N_{images} increase in proportion to the drop radius. An increase in N_{images} can be accomplished by some combination of a decrease in v_z and an increase in the vertical length Z, Eq. (4). However a significant decrease in v_z requires too fine a balance between v_{air} and r^2, Eq. (3). If we keep v_z constant, an increase of Z can be attained by an increase in the number of vertical direction pixels in the CCD array of the camera. Existing CCD cameras with 10 Hz frame reading rates have twice the 736 vertical pixels used in the present camera and larger arrays will probably be available in the future. Therefore based on this consideration alone, drop diameters of several times 20 μm are feasible.

However, there are two problems that must be considered for drop diameters larger than 30 to 40 μm. The dipole force on a drop in a non-uniform electric field is proportional to the third power of the drop diameter. This force was negligible in this experiment, Sec. III C, but would have to be considered for much larger drops. The other problem is that the maintenance of a small and constant v_z, Eq. (3), requires v_{air} to increase as the square of the drop diameter, possibly leading to non-laminar flow. Therefore without more design and experimental studies, our conservative conclusion is that the drop diameter is limited to about 30 μm. This would lead to an increase of the mass search rate by a factor of 3 compared to the 20 μm drops used in this experiment.

2. Increase of drop production rate per column of drops

Let the drop production rate for a column of drops be n per second. Then the vertical separation between drops in a column is $R = v_{air}/n$. The criteria in Sec. IV A 6 require $R > 0.62$ mm. Using $v_{air} = 2.0$ mm/s, this gives an upper limit on n of about 3 Hz. However our experience in this experiment, Sec. II C, strongly suggests that a maximum 1

Hz rate is conservative practice, because of irregularities in drop production.

3. Increase in the number of drop columns

In this experiment we used one column of drops, however the extension to many columns of drops is straightforward. Of course the horizontal separation between adjacent columns must meet the requirements of Eq. (16); a nominal separation of 1 mm is useful for design purposes. The use of multiple columns requires two changes in the experimental design, namely the number of pixels in the horizontal direction in the CCD array must be increased and the space between the electric field plates must be increased. The latter requirement means the alternating potential applied across the plates must also be increased to keep the electric field constant.

Existing 10 Hz frame rate CCD cameras limit the number of columns to three but improvements in these cameras would probably allow five columns. The corresponding increase in the electric plate spacing and the potential difference is straightforward.

4. Correction for drop to drop interactions

It is clear that the primary constraint limiting the density of drops achievable in the measurement chamber is that of Eq. (16). To reiterate, interaction between the drops due to their induced electric dipole moment and viscous coupling requires that there be a minimum separation allowable between drops. In the limit that these interactions are small, both of these effects can be calculated from first principles, for example as in Eq. (15). In principle then, it should be possible to subtract the effect of these perturbing forces from the measured trajectory of each drop. Given this, it would be possible to relax the constraint on R. Since this possibility requires further study, it is not clear to what extent R can be reduced and throughput increased.

5. Summary

Putting these estimates together we can see how to achieve an improvement on the order of 10 times the present mass per second search rate using existing CCD cameras. Future cameras will probably allow a factor of 15 improvement.

---

[1] D. Loomba *et al.*, Rev. Sci. Instrum. **71**, 3409 (2000).

[2] V. Halyo *et al.*, Phys. Rev. Lett. **84**, 2576 (2000).

[3] N.M. Mar *et al.*, Phys. Rev. D **53**, 6017 (1996).

[4] M.L. Savage *et al.*, Phys. Lett. **167B**, 481 (1986).

[5] V.D. Hopper and T.H. Laby, Proc. R. Soc. London **178**, 243 (1941).

[6] W.B. Kunkel, J. Appl. Phys. **21**, 820 (1950); **21**, 833 (1950).

[7] E.R. Lee and M.L. Perl, U.S. Patent 5,943,075, Aug. 24, 1999, Assigned to Stanford University.

[8] The CCD camera, a Cohu 4110, uses the frame transfer method and has digital output.

[9] W.E. Langlois, *Slow Viscous Flow* (Macmillan Company, New York, 1964).

[10] G.S. LaRue *et al.*, Phys. Rev. Lett. **46**, 967 (1981).

[11] M. Marinelli and G. Morpurgo, Phys. Lett. **137B**, 439 (1984).

[12] P.F. Smith *et al.*, Phys. Lett. **153B**, 188 (1985).

[13] W.G. Jones *et al.*, Z. Phys. C **43**, 349 (1989).